III-V compliant substrates implemented by nanocavities introduced by ion implantation

M. Chicoine,[a] C. Beaudoin, and S. Roorda
Regroupement Québécois sur les Matériaux de Pointe (RQMP), Département de Physique, Université de Montréal C.P. 6128 succ. Centre-ville, Montréal, Québec, Canada H3C 3J7

R. A. Masut[b] and P. Desjardins
Regroupement Québécois sur les Matériaux de Pointe (RQMP), Département de Génie Physique, École Polytechnique de Montréal C.P. 6079 succ. Centre-ville, Montréal, Québec, Canada H3C 3A7

(Received 16 July 2004; accepted 6 January 2005; published online 9 March 2005)

A concept for the implementation of a compliant substrate using a buried layer of nanocavities is presented. The purpose of this nanocavity layer is to mechanically decouple a thin substrate layer from the rest of the substrate in order to relax stress in mismatched epilayers. The nanocavities were created by helium implantation in InP(001) followed by thermal annealing under a phosphorous rich atmosphere. Metalorganic vapor phase epitaxy of InAsP/InP heterostructures grown simultaneously on substrates with nanocavities and on conventional substrates were characterized by high-resolution x-ray diffraction, transmission electron microscopy, and optical absorption. It is found that strain relaxation is enhanced for heterostructures grown on substrates with nanocavities and that the dislocations propagate partly in the compliant layer instead of the epilayer. The critical thickness of heterostructures grown on conventional substrates is roughly double that of structures grown on substrates containing nanocavities. © *2005 American Institute of Physics*.
[DOI: 10.1063/1.1863457]

I. INTRODUCTION

Strain can be useful for the design of semiconductor devices because it can be used to modify the band structure by changing the band gap, band-gap offset, and heavy- and light-hole splitting.[1] However, it becomes a limitation for the growth of thick mismatched device structures, as it promotes the formation of misfit dislocations when the elastic energy stored in the epitaxial layer becomes too large. The thickness at which this happens is called the critical thickness (h_c). The misfit dislocations, located at the interface between the substrate and the epitaxial layer, are accompanied by threading dislocations which propagate through the epilayers and limit the quality of the device.[2,3]

There have been numerous attempts to overcome this limitation. One of them is to grow graded buffer layers in which a good proportion of the threading dislocations bend along the interfaces and do not reach the surface.[4,5] However this method requires very thick buffer layers (several microns) and does not totally eliminate threading dislocations.[5] An improvement of this method is to include strained superlattices in the graded buffer layer to further favor dislocation bending.[6,7] Another solution is to grow the epilayers on a compliant substrate, a concept that was introduced by Lo in 1991.[8] The ideal compliant substrate consists of a freestanding substrate thinner than the h_c value associated with the epitaxial layer to be grown on top of it, so that it will adapt its lattice to the overgrown layer lattice instead of relaxing with the formation of threading dislocations. A real life compliant substrate is a thin template layer separated by a "weak" interface or intermediate layer that allows the template to slip on the bulk substrate.[9,10]

Based on straightforward strain-energy considerations, it was generally believed that a compliant substrate would increase the h_c value of the system, as was originally suggested by Lo, but this hypothesis has been criticized by various authors.[11] It has been argued recently that h_c could in fact be lowered because the nucleation barrier for dislocations is lowered, mainly because the drag force on a threading dislocation in a compliant substrate is reduced compared to a misfit dislocation.[12,13] Many experimental approaches to the creation of a weakly coupled layer have been reported in the literature, including amorphous interlayers[14,15] twist-bonded layers,[16,17] and layers of buried nanocavities, produced by post-growth helium or hydrogen implantation.[18–20]

Here, we propose an approach for a compliant substrate based on a uniform layer of buried nanocavities produced by helium implantation *before* growth. The work previously done with nanocavities, as in Refs. 18 and 20, was based on ion implantation carried out *after* the growth of a strained epitaxial layer for the SiGe on Si(001) system. Thus, after thermal annealing, a layer of nanocavities was created and dislocations going from the interface to the nanocavities relaxed strain in the epilayers. This approach is limited to metastable systems with relatively low strain since, otherwise, the strained layer could relax during or immediately after growth, even before the nanocavities are created. In addition, this approach is not advisable for InP-based systems as InP is very sensitive to radiation damage. Our approach, which is more general, is to create a layer of nanocavities before the epitaxial growth, thus decoupling the

[a]Electronic mail: martin.chicoine@umontreal.ca
[b]Presently on sabbatical leave at the Instituto de Ciencia de Materiales de Madrid, 28049 Madrid, Spain.

virtual substrate before growth. Heterostructures were grown simultaneously on InP(001) substrates with nanocavities and on conventional InP(001) substrates. Relaxation and quality of the grown structures were measured by transmission electron microscopy (TEM), high-resolution x-ray diffraction (HRXRD), photoluminescence (PL), and optical absorption measurements.

II. EXPERIMENTAL DETAILS

A. Sample preparation

Three different methods for sample preparation before growth were tested in this work. They involved different parameters and sequences for helium implantation, thermal annealing, and surface treatment. Based on our previous work reported in Ref. 21, the samples were implanted at room temperature with helium at energies varying between 25 and 100 keV at doses, ϕ_{He}, varying between 1 and 3 $\times 10^{16}$ cm^{-2}, procedures known to result in 18 nm wide cavities following a 10 min anneal at 640 °C. The helium beam was focused and scanned over a 1.6×1.6 cm^2 area. The angle of incidence on the target was set to 7° to minimize channeling. The beam current was about 1.5 μA and no significant heating occurred during implantation. The samples were then annealed in a metal organic chemical vapor deposition (MOCVD) reactor under tertiarybutylphosphine (TBP) atmosphere, creating a phosphorous overpressure in order to avoid InP surface degradation. InP/InAsP multiple quantum well structures were grown by MOCVD at 600 °C using TBP, tertiarybutylarsine and trimethylindium as phosphorous, arsenic, and indium sources respectively. A typical InP growth rate was 0.1 nm/s.

For method 1, bare InP(001) substrates were first implanted. They were then thermally annealed to form helium nanocavities. They were then degreased and etched in a 4:1:1 sulfuric acid, deionized water, and hydrogen peroxide solution to prepare the surface for MOCVD growth (this sequence is later referred to as "surface treatment"). Multiple quantum well structures grown on substrates prepared with this method were of very poor quality. The resulting surface morphology was very rough and HRXRD showed no sign of the epilayer.

For method 2, we used InP(001) samples covered with 100 nm of SiO_2 furnished by Nortel Networks in order to protect the surface during ion implantation. After implantation, samples were dipped in a 20% hydrofluoric acid aqueous solution to remove the SiO_2. They then received the surface treatment before being placed in the MOCVD reactor for high temperature annealing and growth. This method gave better results. Surface morphology was acceptable and the epilayers had reasonable structural quality as revealed by HRXRD.

For method 3, the samples with the SiO_2 cap layer were first implanted and then annealed at 620 °C or 640 °C for 10 min and then at 600 °C for another 10 min without the SiO_2 cap being removed. The aim of this annealing sequence was to first create the cavities with the higher temperature anneal and then to reduce the remaining surface defect density with the lower temperature anneal. The SiO_2 cap was then removed by etching in HF, surface treatment was done and samples were put back in the reactor chamber for growth. This method gave the best results. Surface morphology, photoluminescence intensity, and photoluminescence full width at half maximum (FWHM) measured for structures grown on implanted substrates were comparable to those grown on virgin substrates.

B. Characterization

The structural characterization of the heterostructures was carried out using HRXRD and TEM. HRXRD measurements were carried out using the Cu $K_{\alpha 1}$ ($\lambda = 0.15406$ nm) radiation from a Philips high-resolution five-crystal diffractometer with a four-reflection Ge(220) monochromator. A 0.45° receiving slit was placed in front of the detector for $\omega - 2\theta$ rocking curves and triple-axis geometry carried out with a two-reflection Ge(220) analyzer was used for reciprocal space maps measurements. TEM specimens were prepared in cross section with ⟨110⟩ surface normals using standard mechanical polishing followed by room-temperature low-angle (4°) argon ion milling at 5 keV in a Gatan precision ion polishing system. The ion energy was gradually reduced to 2.5 keV during the final stages of thinning to minimize radiation damage to the samples. Images were recorded at 300 kV on a Philips CM30 microscope. Optical absorption and PL measurements were performed at 8 K using a Bomem DA3 Fourier transform infrared spectrometer.

III. RESULTS

A. Structural properties

Figure 1 shows HRXRD $\omega - 2\theta$ curves around the (004) reflection from samples consisting of a $5 \times$(InP/InAsP) heterostructure grown simultaneously on a substrate with nanocavities (curve a) and, for reference, on a virgin substrate (curve b). The nanocavities were created with $\phi_{He} = 3 \times 10^{16}$ cm^{-2} at 25 keV and annealing at 620 °C for 10 min. Those implantation and annealing parameters lead to nanocavities with diameters from 4 to 15 nm.[21] The substrate peaks are situated at zero relative angle. The two curves differ notably in their zero-order superlattice peak position (related to the InAsP composition, indicated by arrows) and satellite spacing (related to the period of the quantum well structure). Those differences between the two samples could be attributed to growth nonhomogeneity in the MOCVD reactor. The spacing of the satellite peaks was used to deduce the period of the structures. The composition in the InAsP layers, as well as the relaxation of the structures, was deduced from reciprocal space maps. From this information, the structure of the samples from curves a and b were determined to be $5 \times$(10 nm $InAs_{0.275}P_{0.743}$/20 nm InP) layers covered with a 102 nm InP cap layer, and $5 \times$(9.5 nm $InAs_{0.25}P_{0.75}$/18 nm InP) layers covered with a 97 nm InP cap layer, respectively. Both samples had a $\approx$50 nm InP buffer layer. We chose to use a small buffer layer thickness so that the bottom of the heterostructure would be as near as possible to the nanocavities. Simulated HRXRD scans, based on the fully dynamical formalism of

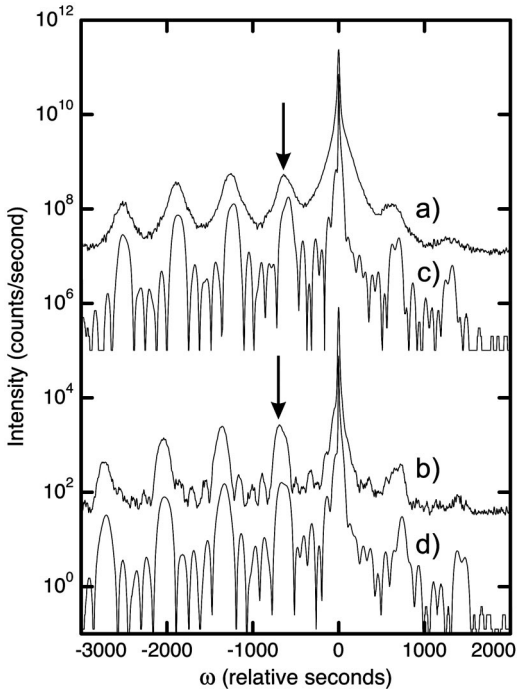

FIG. 1. $\omega-2\theta$ patterns around the 004 reflection for heterostructures grown on (a) an InP(001) substrate implanted with $\phi_{He}=3\times10^{16}$ cm^{-2} implantation at 25 keV and preannealed 10 min at 620 °C and (b) a conventional substrate. Arrows indicate the position of the zero-order superlattice peak position. Simulations are also shown below the measured curves (curves c and d). The curves are vertically shifted for clarity.

Tagaki[22] and Taupin[23] are also shown in Fig. 1 for comparison (curves c and d). The simulations were carried out assuming perfectly abrupt and coherent interfaces with linearly interpolated elastic constants. The simulation to curve a takes into account the 2.3% relaxation that was measured from the reciprocal space map (see below). The measured and simulated curves in Figs. 1(a) and 1(b) are in excellent agreement with respect to the angular position and relative intensities of both the diffraction peaks and the interference fringes.

Comparing the curve from the sample grown on an implanted substrate (curve a) to its simulated curve and to the curve from the sample grown on a conventional substrate, (curve b) in Fig. 1, also shows that samples grown on the implanted substrate have broader satellite peaks and less fine structure, i.e., the finite thickness interference fringes disappear. The same situation, loss of the fine structure in the HRXRD curve, is observed for all samples grown on implanted substrates, which is probably due to microscopic interface roughness and significant plane bending near the interfaces.[24] A possible factor which could contribute to this loss and to the broadening of the satellite peaks in the HRXRD curves is the microscopic nonuniformity of the nanocavities layer, resulting in a spatially nonuniform local relaxation of the heterostructure strain.

In order to compare the relaxation behavior in samples grown on substrates with and without nanocavities, we measured the relaxation ratio R for a series of samples. It is defined by

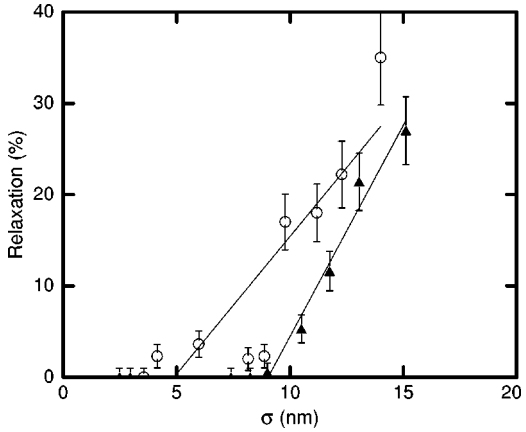

FIG. 2. Relaxation of heterostructures grown on InP(001) virgin substrates (▲) and substrates implanted with $\phi_{He}=3\times10^{16}$ cm^{-2} at 25 keV and preannealed 10 min at 620 °C (○). The continuous lines are linear fits to the nonzero values for each data set.

$$R=\frac{a_{\parallel}-a_s}{a_r-a_s}, \tag{1}$$

where $a_{\parallel}$ is the in-plane lattice parameter of the heterostructure, a_s is the substrate lattice parameter and a_r is the equivalent cubic lattice parameter which corresponds to the lattice parameter of a completely relaxed double layer. It is derived from elasticity theory and is given by

$$a_r=a_{\perp}\left(\frac{1-\nu}{1+\nu}\right)+2a_{\parallel}\left(\frac{\nu}{1+\nu}\right), \tag{2}$$

where $a_{\perp}$ is the average lattice parameter of a double layer composed of one InAsP and one InP layer, and ν is the average Poisson ratio of the double layer, which is interpolated between that of InP ($\nu_{InP}=0.361$) and InAs ($\nu_{InAs}=0.354$) for the InAsP composition expected from the growth conditions. The in-plane and out-of-plane lattice parameters are obtained either from a reciprocal space map or from (115) and $(\overline{115})$ asymmetrical reflections. Measurements in orthogonal azimuthal directions gave consistent $a_{\perp}$ values and indicated some slight anisotropy in the relaxation with respect to ⟨110⟩ directions. The average relaxation was used.

The relaxation ratio for the sample grown on a conventional substrate [Fig. 1(a)] and that on a substrate with nanocavities [Fig. 1(b)] were ≈0% and 2.3%, respectively, showing that h_c is lowered for substrates with nanocavities, in agreement with the model of Kästner and Gösele.[12,13] The relaxation was also measured for a series of samples with various thicknesses and mean mismatch values grown simultaneously on virgin substrates and on substrates with nanocavities placed side by side in the reactor. It is expressed as a function of the quantity $\sigma=nfh$, where n is the number of periods in the structure, $f=(a_r-a_s)/a_s$ is the misfit strain relative to the InP substrate and h is the thickness of one InAsP layer. The results are shown in Fig. 2 for InAsP/InP heterostructures grown on virgin substrates (▲) and substrates with nanocavities (○). Error bars are evaluated by inspection of the HRXRD reciprocal space maps. Relaxation for structures grown on implanted substrates is consistently

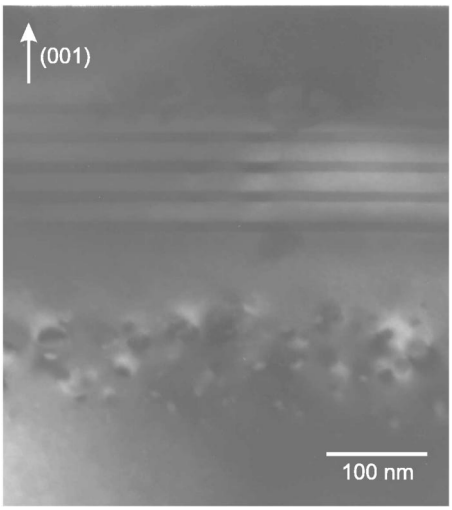

FIG. 3. TEM micrograph of same sample as in Fig. 1(a) with g near the $00\bar{2}$ orientation.

2% to 5% higher than those grown on conventional substrates. Linear fits of the nonzero relaxation values for each set of data (continuous lines shown in the figure) cross the σ axis at 4.9 nm in the case of implanted substrates and at 9.1 nm in the case of conventional substrates, showing that h_c for structures grown on conventional substrates is roughly 185% of h_c for structures grown on substrates containing nanocavities. The data for the substrates with nanocavities are not very well described by a linear fit.

A cross-sectional TEM image from the same sample as in Fig. 1(a) (grown on a substrate with nanocavities), shown in Fig. 3 indicates that interfaces are sharp and uniform with no evidence of dislocations in the multilayer. The imaging conditions used in this figure prevent from viewing misfit dislocations but inspection at other imaging conditions, while showing dislocations in the nanocavity area, showed no evidence of misfit dislocations. This is surprising because, as HRXRD indicates, the structure is partially relaxed.

For samples with higher strain relaxation, dislocations start to appear. Figure 4 shows a micrograph of a heterostructure that consists of a 50 nm InP buffer layer and 10 $\times$(6.4 nm $InAs_{0.38}P_{0.62}$/16 nm InP), with $\sigma \approx 6$ nm. The measured relaxation of this sample is 3.5% while the same structure grown on a conventional substrate [with structure $10\times$(6.3 nm $InAs_{0.378}P_{0.622}$/15.8 nm InP)] is not relaxed. The micrograph shows that the structure has relaxed by forming dislocations threading through the heterostructure but also between the cavities region and the bottom of the heterostructure. The fact that in this micrograph, a dislocation in the layers is located near dislocations in the buffer layer was only observed at this position of the sample and thus appears to be a coincidence.

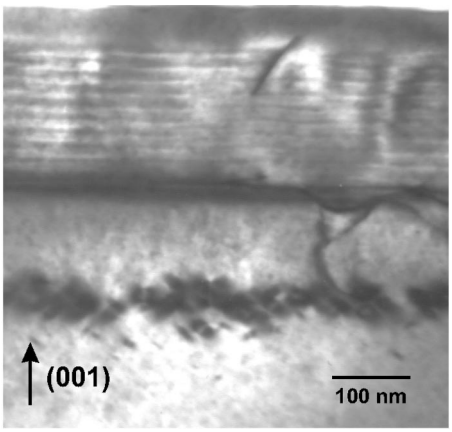

FIG. 4. TEM micrograph ($g=00\bar{2}$) of a heterostructure that has relaxed by forming a dislocation between the cavities region and the bottom of the heterostructure.

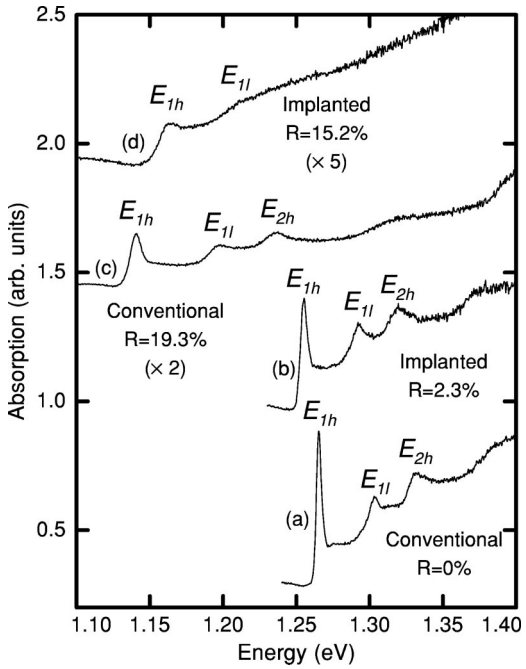

FIG. 5. Low-temperature (8 K) optical absorption for two different structures each grown on a conventional substrate and an implanted substrate. The relaxation value is indicated. The samples consist of (a) 15 $\times$(9.2 nm $InAs_{0.167}P_{0.833}$/12.9 nm InP) grown on a conventional substrate, (b) $15\times$(10.9 nm $InAs_{0.158}P_{0.842}$/12.3 nm InP) grown on an implanted substrate, (c) $15\times$(9.5 nm $InAs_{0.30}P_{0.70}$/11.6 nm InP) grown on a conventional substrate, and (d) $15\times$(10.2 nm $InAs_{0.281}P_{0.719}$/12.4 nm InP) grown on an implanted substrate.

B. Optical properties

The low temperature optical absorption spectra of the samples were also measured. It was found that moderately relaxed samples on compliant substrates retained relatively good optical properties while they deteriorated for higher values of relaxation. Figure 5 shows optical absorption for structures consisting of $15\times$(9.2 nm $InAs_{0.167}P_{0.833}$/12.9 nm InP) grown on a conventional substrate (a) and 15 $\times$(10.9 nm $InAs_{0.158}P_{0.842}$/12.3 nm InP) grown on an implanted substrate (b). The measured relaxations for those samples were 0% and 2.3%, respectively. Optical absorption for more relaxed structures is also shown: 15 $\times$(9.5 nm $InAs_{0.30}P_{0.70}$/11.6 nm InP) grown on a conventional substrate (c) and $15\times$(10.2 nm $InAs_{0.281}P_{0.719}$/12.4 nm InP) grown on an implanted substrate (d). At least three well-resolved transitions are observed in curves (a)–(c) and two in the case of curve (d). The peaks are labeled as

follows: E_{nh} represents a transition between the nth quantized levels in the heavy-hole valence and conduction bands and E_{nl} represents a transition between the nth quantized levels in the light-hole and conduction bands. The differences in peak positions for samples grown on implanted and nonimplanted substrates stem from the differences in composition and thickness of the layers. Lower transition energies are obtained with thicker quantum wells because the energy levels are less confined. A higher As concentration in an InAsP well leads to more strain and thus to a larger heavy- and light-hole bands splitting, so that transitions involving the heavy-hole band shift to lower energies and transitions involving the light-hole band shift to higher energies.Relaxation has the effect of reducing strain and thus reducing heavy- and light-hole bands splitting.[25]

The figure shows that the structures grown on compliant substrates show excitonic absorption peaks with larger FWHM and lower oscillator strength than those grown on conventional substrates. The FWHM is, in general, double the FWHM of the same structure grown on a conventional substrate and, for example, 8 meV compared to 4 meV for the lower energy peak of curves (a) and (b).

IV. DISCUSSION

It is seen from Fig. 2 that relaxation was more efficient for heterostructures grown on substrates with nanocavities. This is in agreement with the theoretical work done by Kästner and Gösele (see Refs. 12 and 23) where they argued that the critical thickness of a structure grown on a compliant substrate should be lower than one on a conventional substrate. In their model, based on the Matthews–Blakeslee model,[26,27] misfit dislocations usually observed in plastically relaxed conventional substrates are replaced by slip steps in the intermediate layer between the rigid substrate and the template. Slip steps are energetically more favorable than misfit dislocations, which explains why h_c is lowered with compliant substrates. In our case, the slip steps would be located in the cavity layer and could probably not be discerned from the dislocations already present in this region. The model of Kästner and Gösele predicts a critical thickness reduced by a factor of the order of 2, which is in agreement with the factor 1.8 found in this work.

Another feature of the Kästner and Gösele model is that dislocations are attracted by an image force in the template layer instead of being driven to the sample surface as threading dislocations.[12,28] In our samples, where the nanocavity layer played the role of the intermediate layer, dislocations were likely to end at the surface of a nanocavity or in dislocation loops. This was observed in samples with higher total misfit strains as is seen in Fig. 4. In this figure, it appears that strain was relieved by dislocations threading through the heterostructure but also going to the implanted region. The fact that relaxation occurs partly by formation of threading dislocations ending in the cavity region implies that the areal density of threading dislocations in the heterostructure itself is reduced, which would be beneficial for the optical properties of the quantum well structure. It is not clear what the strain relief mechanisms were in the samples with lower strains, as no dislocations were observed in those samples, even if they were partially relaxed. One possible explanation is that the InP layer between the bottom of the quantum wells and the nanocavities layer was at least partially mechanically decoupled from the substrate because of the nanocavity layer. This would mean that strain was partitioned between the InP layer and the In–AsP/InP multiple quantum wells, so that the strain of the heterostructure itself was reduced. We looked for a consequence of this on the XRD near the substrate peak, but were unable to find any clear evidence of it, probably because the contribution for such a thin weakly relaxed InP layer is low and spread in a wide angular span.

Finally, we note the slightly deteriorated structural and optical quality of structures grown on implanted compliant substrates compared to those grown on virgin substrates. This can be seen with HRXRD measurements where the fine structure of the curves was lost, which was attributed to microscopic interface roughness. The broader satellite peaks from implanted samples could also stem from the nonuniformity of the nanocavity layer, resulting in a spatially nonuniform relaxation. More evidence for this interface roughness is found from the increased FWHM of optical absorption peaks, although the overall optical properties remained reasonably good.

V. CONCLUSION

In conclusion, we have found parameters to grow relatively good quality epitaxial MQW structures on He-implanted and annealed InP(001) compliant substrates. It is shown that the value of the critical thickness is reduced for structures grown on He-implanted InP(001) compliant substrates compared to conventional InP(001) substrates, as predicted by the model of Kästner and Gösele. High-strain heterostructures grown on compliant substrates were relaxed by threading dislocations going through the heterostructure, but also by dislocations going to the nanocavities layer. For moderately strained heterostructures, no dislocations are observed to produce relaxation, whose mechanism remains so far undetermined.

The overall quality of the structures grown by the method presented in this article was inferior to equivalently relaxed structures grown on conventional substrates, as seen in HRXRD and optical absorption measurements. Choosing this method to grow thick relaxed layers while minimizing the introduction of dislocations will require further work to understand the exact relaxation mechanism and thus achieve higher quality heterostructures on compliant substrates.

ACKNOWLEDGMENTS

The authors are grateful to Réal Gosselin and Pierre Bérichon for their technical assistance. This work benefitted from grants from the NSERC of Canada and FCAR of Québec. P. D. thanks the Canada Research Chair program for financial support. R.A.M. acknowledges the financial assistance (SAB2003-0159) of the Ministerio de Educacion y Ciencia of Spain.

[1]M. Beaudoin, A. Bensaada, R. Leonelli, P. Desjardins, R. A. Masut, L. Isnard, A. Chennouf, and G. L'Espérance, Phys. Rev. B **53**, 1990 (1996).
[2]F. M. Ross, R. Hull, D. Bahnck, J. C. Bean, L. J. Peticolas, and C. A. King, Appl. Phys. Lett. **62**, 1426 (1993).
[3]P. Kozodoy, J. P. Ibbetson, H. Marchand, P. T. Fini, S. Keller, J. S. Speck, S. P. DenBaars, and U. K. Mishra, Appl. Phys. Lett. **73**, 975 (1998).
[4]K. Tominaga, M. Hosoda, N. Ohtani, T. Watanabe, H. Inomata, and K. Fujiwara, J. Appl. Phys. **80**, 5915 (1996).
[5]L. M. Giovane, H.-C. Luan, A. M. Agarwal, and L. C. Kimerling, Appl. Phys. Lett. **78**, 541 (2001).
[6]M. E. Givens, J. J. Coleman, C. A. Zmudzinski, R. P. Bryan, M. A. Emanuel, and L. M. Miller, J. Appl. Phys. **63**, 5092 (1988).
[7]W. T. Masselink, M. V. Klein, Y. L. Sun, Y. C. Chang, R. Fischer, T. J. Drummond, and H. Morkoç, Appl. Phys. Lett. **44**, 435 (1984).
[8]Y. H. Lo, Appl. Phys. Lett. **59**, 2311 (1991).
[9]G. Kästner and U. Gösele, J. Appl. Phys. **88**, 4048 (2000).
[10]K. Vanhollebeke, I. Moerman, P. Van Daele, and P. Demeester, Prog. Cryst. Growth Charact. Mater. **41**, 1 (2000).
[11]See Ref. 12 and references therein.
[12]G. Kästner and U. Gösele, Appl. Phys. Lett. **82**, 3209 (2003).
[13]G. Kästner, Phys. Status Solidi A **195**, 367 (2003).
[14]F. K. LeGoues, A. R. Powell, and S. S. Iyer, J. Appl. Phys. **75**, 7240 (1994).
[15]M. A. Chu, M. O. Tanner, F. Huang, K. L. Wang, G. G. Chu, and M. S. Goorsky, J. Cryst. Growth **175–176**, 1278 (1997).
[16]F. E. Ejeckam, Y. H. Lo, S. Submaranian, H. Q. Lou, and B. E. Hammons, Appl. Phys. Lett. **70**, 1685 (1997).
[17]P. Kopperschmidt, S. Senz, R. Scholz, and U. Gösele, Appl. Phys. Lett. **74**, 374 (1999).
[18]B. Holländer, S. Lenk, S. Mantl, H. Trinkaus, D. Kirch, M. Luysberg, T. Hackbarth, H. J. Herzog, and P. F. P. Fichtner, Nucl. Instrum. Methods Phys. Res. B **155–157**, 357 (2001).
[19]B. Holländer, S. Mantl, R. Liedtke, S. Mesters, H. J. Herzog, H. Kibbel, and T. Hackbarth, Nucl. Instrum. Methods Phys. Res. B **148**, 200 (1999).
[20]H. Trinkaus, B. Holländer, S. Rongen, S. Mantl, H. J. Herzog, J. Kuchenbecker, and T. Hackbarth, Appl. Phys. Lett. **76**, 3552 (2000).
[21]M. Chicoine, S. Roorda, R. A. Masut, and P. Desjardins, J. Appl. Phys. **94**, 6116 (2003).
[22]S. Tagaki, Acta Crystallogr. **15**, 1311 (1962).
[23]D. Taupin, Bull. Soc. Fr. Mineral. Cristallogr. **87**, 469 (1964).
[24]P. Desjardins, H. Marchand, L. Isnard, and R. A. Masut, J. Appl. Phys. **81**, 3501 (1997).
[25]R. Y.-F. Yip, A. Aït-Ouali, A. Bensaasa, P. Desjardins, M. Beaudoin, L. Isnard, J. L. Brebner, J. F. Currie, and R. A. Masut, J. Appl. Phys. **81**, 1905 (1997).
[26]J. W. Matthews, S. Mader, and T. Light, J. Appl. Phys. **41**, 3800 (1970).
[27]J. W. Matthews and A. E. Blakeslee, J. Cryst. Growth **27**, 118 (1974).
[28]R. V. Kukta and L. B. Freund, Mater. Res. Soc. Symp. Proc. **535**, 3 (1999).